SUPPLEMENTARY INFORMATION

Materials and Methods

Histological analyses.

All biopsy specimens were fixed in formaldehyde 10% for 6h and paraffin embedded. Thin sections of 3 microns were stained with hematoxylin-eosin (HE), periodic acid-Schiff (PAS), Masson trichromic and with methenamine silver. A small fragment with cortical areas was cryopreserved and processed for immunofluorescence staining using fluorescein-labelled antibodies: anti-IgA, IgG, IgM, C3, C1q, C4, fibrinogen, albumin and anti-kappa, anti-lambda. (DAKO). For EM studies, a small piece was fixed in 2.5% glutaraldeyide (pH 7.4), then in osmium tetroxide, and finally embedded in Spurr resin. Carefully selected areas were studied in 1 micron sections stained with toluidine blue. Specimens were observed in a Philips M2085 transmission EM**.**

Purification of complement components and activation fragments.

fH and fB were purified from plasma of healthy donors by a two-step method. First, filtered plasma was applied to a 5 ml affinity column to which 10mg of mouse anti-human fH mAb or anti-human fB mAb was coupled. Bound protein was eluted at low pH and fractions containing fH or fB were pooled and dialysed against Hepes buffer (10 mM Hepes, pH 7.4 100 mM NaCl). fH and fB preparations were polished by gel filtration on a SuperoseTM 6 10/300 column (GE Healthcare). Factor B and fH used in biacore experiments were polished on a Superdex 200 column in HBS/Mg/P buffer (10mM Hepes pH7.4, 150mM NaCl, 1mM MgCl2, 0.005% surfactant P20) just prior to use. Preparations of fH or fB were obtained without any detectable contaminants or aggregates. Purity was confirmed by sodium dodecyl sulfate polyacrylamide gel electrophoresis (SDS-PAGE). Concentrations of purified proteins were assessed using absorbance at A280, molarities were calculated using a extinction coefficient for fH of 1.95 (1) and of 1.25 for fB (2).

C3 was prepared from plasma containing 20 mM EDTA and 10mM benzamidine. Supernatant of a 10% sodium sulphate precipitation, dialysed against 50 mM phosphate buffer, pH 7, containing 5mM benzamidine, 10mM EDTA and 150mM NaCl, was applied to a lysine-sepharose column. The flow through was collected, dialysed against 20 mM Tris buffer, pH 8.6 and applied to a DEAE-Sepharose anion exchange column.

Protein was fractionated using a gradient to 0.35M NaCl, C3-containing fractions were identified by ELISA, dialyzed against 20mM Na phosphate pH 6, 40mM NaCl and applied to a Mono S HR 5/5 cation exchange column (GE Healthcare). Protein was eluted with a gradient to 0.5M NaCl. C3-containing fractions were pooled and preserved frozen at -70ºC. C3b was generated by limited digestion with trypsin as previously described (3) and re-purified on a Mono Q HR 5/5 column (GE Healthcare). Both C3 and C3b preparations were polished by gel filtration on a SuperoseTM 6 10/300 column (GE Healthcare) before being used to eliminate any detectable contaminants or aggregates. C3(H2O) was generated by 3h incubation at 37ºC in a 20mM Na/K phosphate pH6, 100mM NaCl buffer containing 0.33 M potassium isothiocyanate (4) and gel filtration on a 5ml Sephadex G25 desalting column equilibrated with 20mM Tris pH 7.6; 150 mM NaCl buffer.

Factor I was purchased from Comptech (Tyler) or a generous gift of Dr. R. Sim (MRC Immunochemistry Unit, Oxford University, Oxford, United Kingdom). Factor D (fD) was purchased from Calbiochem (Merck) or from Comptech. Recombinant soluble MCP (sMCP) and soluble DAF (sDAF) were gifts of Prof. Susan Lea (Oxford, United Kingdom).

Proteomic analyses

Aliquots from the MonoS chromatography peaks containing C3 were loaded onto a 10% SDS-PAGE gel and stained with Coomassie Brilliant Blue R-250 (BioRad). α-chains of C3 were excised from the gel automatically in a Proteomeworks Plus Spot Cutter System (BioRad), deposited in 96-well polypropylene reaction plates and digested automatically using a DigestPro MS (Intavis AG), the digestion protocol based on Shevchenko et al (5) with minor variations. Tryptic peptides were eluted, dried in a speed-vacuum and resuspended in 4 µl 30% acetonitrile (ACN) and 0.1% trifluoroacetic acid (TFA). One microliter was then deposited onto a 800 mm AnchorChip MALDI probe (Bruker-Daltonics), allowed to dry at RT, covered by 1µl aliquot of matrix solution (3 mg/mL of α-cyano-4-hydroxycinnamic acid (Bruker-Daltonics) in 33% ACN and 0.1 %TFA) and allowed again to dry at RT. For MALDI-TOF/TOF analysis, samples were automatically analyzed in an Autoflex Smartbean TOF/TOF mass spectrometer (Bruker-Daltonics) equipped with a LIFT ion selector and a Reflectron ion reflector. Typically, 1000 scans for peptide mass fingerprint (PMF) and 2000 scans for MS/MS were collected. Automated analysis of mass data was performed using

flexAnalysis software (Bruker-Daltonics). PeptideMass (http://www.expasy.ch/tools/peptide-mass.html) from the ExPASy proteomic server was used for determining the expected differences in the peptide fingerprinting between the α-chains of C3WT and C3923ΔDG that allowed us to determine which protein was present in each peak. Spectra were submitted to Mascot (Matrix Science) and BLAST database searches for confirmation of results.

Electron microscopy and 3D reconstruction

Purified $C3_{WT}$ and $C3_{923\Delta DG}$ in 25mM TrisHCl pH8.0, 50mM NaCl were applied to carbon-coated grids and negatively stained with 1% uranyl formate. Observations were performed in a JEOL 1230 electron microscope operated at 100kV and micrographs were recorded at a nominal magnification of 50,000 under low dose conditions. Micrographs were digitized and averaged to 4.2Å/pixel and the contrast transfer function estimated using CTFFIND3 (7) and corrected by flipping phases. Around 6000 images of molecules for each specimen were extracted and refined using EMAN (3). Reference-free averages were obtained using EMAN and maximum likelihood (4). The three-dimensional reconstruction was obtained using angular refinement methods in EMAN (8), testing two distinct templates as initial reference for refinement, both of which provided the same final solution. One template was built by low-pass filtering the atomic structure of C3 (PDB file 2A73) (9) to very low resolution (> 60 Å) whereas a second template was a featureless noisy Gaussian blob constructed using EMAN to remove the bias from the initial reference. Images of individual molecules collected for $C3_{WT}$ and $C3_{923\ DG}$ were processed independently, and in both cases, the data set revealed that molecule images covered adequately the Euler angles. The resolution of the maps was estimated to be ~25Å for both structures by Fourier Shell Correlation using the criteria of a correlation coefficient of 0.5. The absolute handedness of the reconstructions was defined by fitting of the atomic structure of the C3 into the EM maps using ADP_EM (10).

References for supplementary Materials and Methods:

1. Hakobyan S, Harris CL, Tortajada A, Goicochea de Jorge E, Garcia-Layana A, Fernandez-Robredo P, Rodriguez de Cordoba S, Morgan BP. Measurement of Factor H Variants in Plasma Using Variant-Specific Monoclonal Antibodies: Application to Assessing Risk of Age-Related Macular Degeneration. *Invest Ophthalmol Vis Sci*. 2008;49(5):1983-1990.
2. Tortajada A, Montes T, Martinez-Barricarte R, Morgan BP, Harris CL, Rodríguez de Cordoba S. The disease-protective complement factor H allotypic variant Ile62 shows increased binding affinity for C3b and enhanced cofactor activity. *Hum Mol Genet.* 2009;18(18):3452-3461.
3. Sánchez-Corral P, Antón LC, Alcolea JM, Marqués G, Sánchez A, Vivanco F. Separation of active and inactive forms of the third component of human complement, C3, by fast protein liquid chromatography (FPLC). *J Immunol Methods*. 1989;122(1):105-113.
4. Pangburn M, Schreiber R, Müller-Eberhard H. Formation of the initial C3 convertase of the alternative complement pathway. Acquisition of C3b-like activities by spontaneous hydrolysis of the putative thioester in native C3. *J Exp Med.* 1981;154(3):856-867.
5. Shevchenko A, Tomas H, Havlis J, Olsen JV, Mann M. In-gel digestion for mass spectrometric characterization of proteins and proteomes. *Nat Protoc.* 2007;1(6):2856-2860.
6. Janssen BJC, Huizinga EG, Raaijmakers HCA, Roos A, Daha MR, Nilsson-Ekdahl K, Nilsson B, Gros P. Structures of complement component C3 provide insights into the function and evolution of immunity. *Nature.* 2005;437(7058):505-511.
7. Mindell JA, Grigorieff N. Accurate determination of local defocus and specimen tilt in electron microscopy. J Struct Biol. 2003;142(3):334-347.
8. Ludtke SJ, Baldwin PR, Chiu W. EMAN: Semiautomated Software for High-Resolution Single-Particle Reconstructions. J Struct Biol. 1999;128(1):82-97.
9. Scheres SHW, Valle M, Carazo JM. Fast maximum-likelihood refinement of electron microscopy images. Bioinformatics. 2005;21(Suppl 2):ii243-244.

10. Garzon JI, Kovacs J, Abagyan R, and Chacon P. ADP_EM: fast exhaustive multi-resolution docking for high-throughput coverage. Bioinformatics. 2007;23(4):427-433.

Supplementary Table I

Primers for the PCR amplification of *C3*

Primer	Forward	Reverse
C3-E1	TCCCAGCCTACAGAGAGATTCCT	CCAAATGTCTGCTTCCACCC
C3-E2	TGGGAGTCATGGTGGCTGCT	TTCAGTGGGAGGGACTTAGAGGG
C3-E3,4	TCGCACCTCCTTCACATGCC	CCCTTCCGGTGTGTCTTTCTCTG
C3-E5,6,7	CCCACCTGGGTCCCTGTTCT	CCTGGTCTTCACCTGGTCCCT
C3-E8, 9	GCCAGGTGAGAGGCCAGCAG	CCCTCTCAGACTGGGCCTACCC
C3-E10, 11	GAAGTTGGGGTCCATTCTGAGGG	GTTTCCTCAAACTGCGGACCC
C3-E12, 13	CACCAATTCCCAGGTCTCAGGG	GCGAGCCCAGGGCACACTTA
C3-E14	AGCACCCACTCCATCCCAGG	CCCAATTGGAACCCATGTCCA
C3-E15,16,17	TCACGGAGAAGCGAATGGAC	CAGACAGGGGCCTCCTCCC
C3-E19,20	GGCCTCCCTAAGTGCTGGGATT	GCCATCGAGGCTGGCCCTCT
C3-E20,21	GGCTTCAGCAAAGACAGGCTGA	GGGACTTCCAAATTTCCTAAGCTGG
C3-E22,23	GGACAGTGCCCTGCTGACCA	CAGATGGGCTGTTCTAGCTGAAGG
C3-E24	CCCTGTGAAGCACCTCCCAC	AGGGCCTCAGAGGGCGTAGC
C3-E25,26	CCACCTCCTCGTTCTGATCCC	TGGAGTGACGCCTCTGGCTC
C3-E27	TGACCTTCCTAGGGTAGCGGG	GCAGTGATGTCTGTTATTGCACTGG
C3-E28,29	TGCAGCAACAAGGCAGCTCA	CCTGAACCTGGGCCCTGAGA
C3-E30,31,32,33	CCACTTTCCCAGGCTCCCAG	GCAAAGCAAGGACTGTCTGTGTTG
C3-E34,35	CCCTCTGTGCTGCTATGTGGGA	GACCCTGTCTCCTCTGGCCC
C3-E36	CAGCTCCCAAGACAATGCTGG	TCAGACCCGTGGGACCTTCA
C3-E37,38	GCCTGCGTGTCCCAGGAATC	ACAGCCACCCACGCAATGAT
C3-E39,40,41	TGGGCCATAGTGTGACTGGCT	GCTGTGAGCTGCCGGTGAGT

Supplementary Figure 1

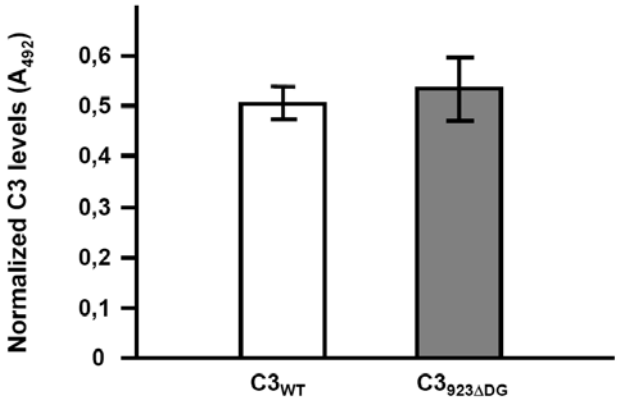

$C3_{923\Delta DG}$ express normally in CHO cells

Figure shows levels of $C3_{WT}$ (white) and $C3_{923\Delta DG}$ (grey) in the supernatants of CHO transfected cells. To express these recombinant C3 mutants, a cDNA encoding full length C3 (C3-cDNA) was introduced in the eukaryote expression vector pCI-Neo (Promega). The c.2767-2774delACGGTG mutation was introduced in the C3-cDNA by using QuickChange site-directed mutagenesis kit (Stratagene) and appropriate primers. All clones were sequenced in their entirely to confirm a correct DNA sequence. CHO cells were maintained in HAM F12 medium (GIBCO-BRL) supplemented with 10% fetal calf serum, L-glutamine (2 mM final concentration), penicillin and streptomycin (10 U/ml and 100 µg/ml). Transient transfections were performed in triplicate using Lipofectine (Invitrogen) as recommended by the manufacturer. Cells were plated in p60 plates 1 day prior to transfection at 3 x 10^5 cells per well. Transfections were carried out with 5 µg of either $C3_{WT}$ or $C3_{923\Delta DG}$ pCI-Neo constructs and 5 µg of a fB pCI-Neo construct (as a transfection control for normalization) mixed with 24 µl of Lipofectine in a total volume of 1 ml of medium per well. C3 and fB concentrations in the supernatants were quantified by a sandwich ELISA similar to that described for fH (1).

1. Hakobyan S, Harris CL, Tortajada A, Goicochea de Jorge E, Garcia-Layana A, Fernandez-Robredo P, Rodriguez de Cordoba S, Morgan BP. Measurement of Factor H Variants in Plasma Using Variant-Specific Monoclonal Antibodies: Application to Assessing Risk of Age-Related Macular Degeneration. Invest *Ophthalmol Vis Sci.* 2008;49(5):1983-1990.

Supplementary Figure 2

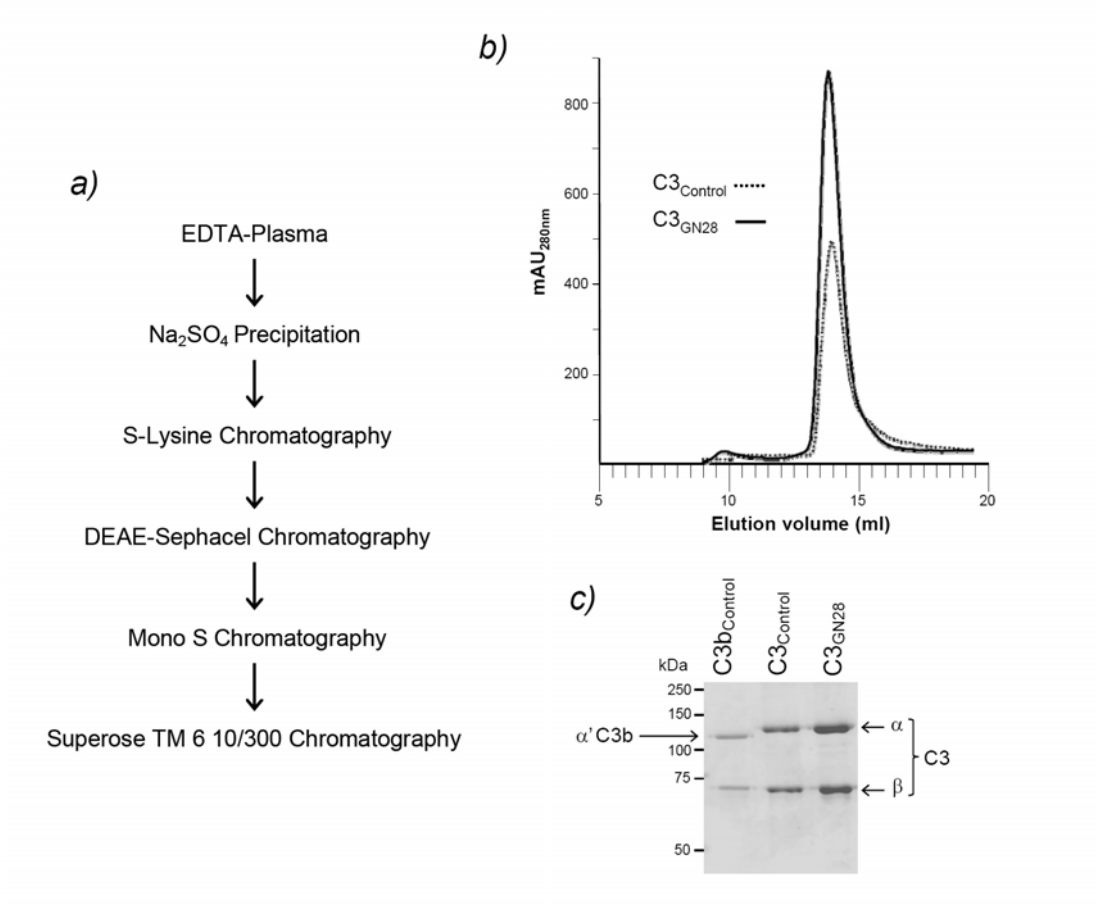

Purification of C3 from patients and controls.

C3 was purified from the plasma of controls (dashed line) and GN28 (heterozygote carrier of the p.923DelAspGly mutation; solid line) as described in materials and methods and illustrated as a flow diagram in (a). A polishing step of gel filtration on a SuperoseTM 6 10/300 column (GE Healthcare) was included to remove aggregates (b). Fractions containing C3 were pooled and stored frozen at -70ºC. C3 purity of the final preparations was confirmed by SDS-PAGE under reducing conditions. Preparations of C3 from controls and GN28 were obtained without any detectable contamination of C3b (c).

Supplementary Figure 3

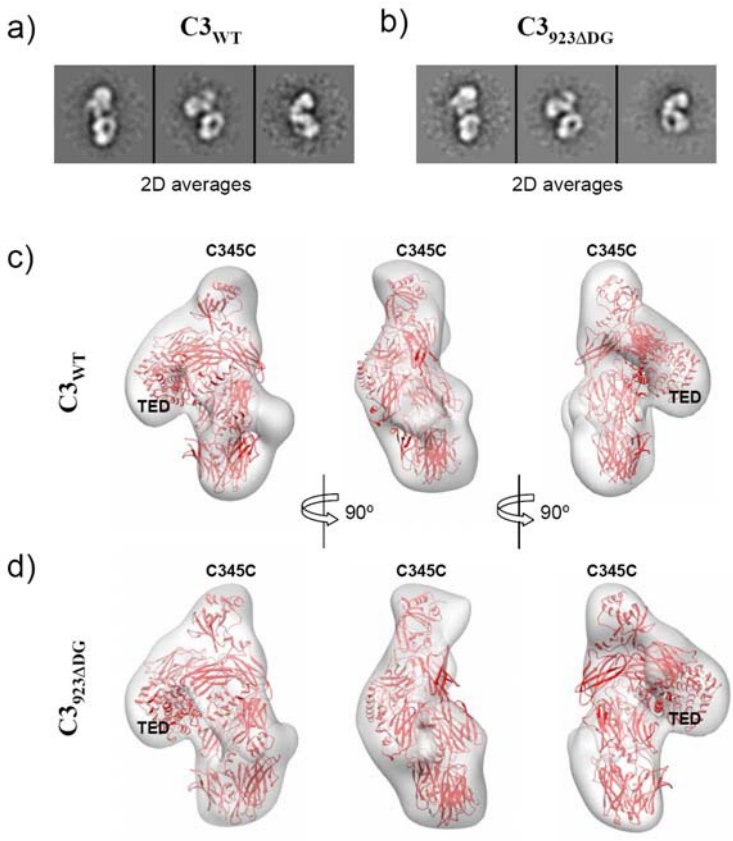

Electron microscopy and 3D reconstruction of $C3_{WT}$ and $C3_{923\Delta DG}$

a) A gallery of selected reference-free 2D averages of the data set obtained for $C3_{WT}$ revealing different shapes corresponding to distinct views of the molecule.

b) A gallery of selected reference-free 2D averages of the data set obtained for $C3_{923\ DG}$ depicting similar structural features to those obtained for $C3_{WT}$.

c) Three views of the 3D reconstruction of $C3_{WT}$ at a resolution of 25Å represented as a gray transparent density. The atomic structure of C3 (PDB file 2A73) (1) (red ribbons) was computationally fitted within the EM structure revealing the close agreement between the atomic and EM structures, and permitting the assignment of domains in the EM reconstruction.

d) Three views of the 3D reconstruction of $C3_{923\ DG}$ at a resolution of 25Å represented as a gray transparent density. The fitting of the atomic structure of C3 (PDB file 2A73) (1) (red ribbons) into this EM structure indicates that the mutation does not induce significant conformational changes that can be detected at this resolution.

Supplementary Figure 4

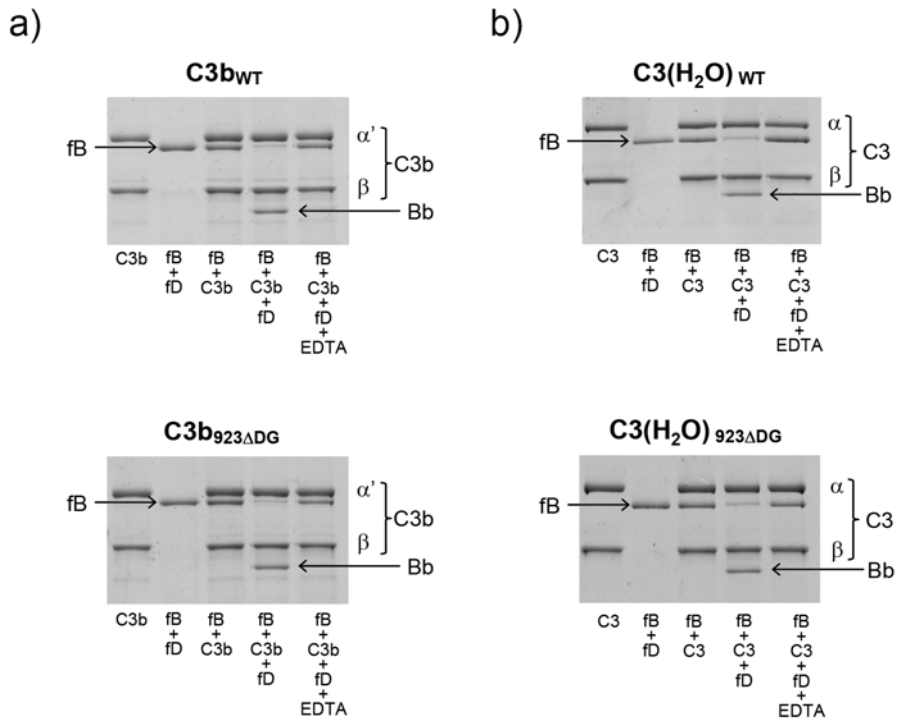

C3b$_{923\Delta DG}$ and C3(H$_2$O)$_{923\Delta DG}$ interact with and consume fB in the presence of fD and Mg2+.

C3$_{923\Delta DG}$ and C3$_{WT}$ were purified to homogeneity from plasma of GN28 and a control individual. Each C3 was either hydrolysed (b) using potassium isothiocyanate or cleaved to C3b with trypsin (a), before incubation with factors B and D as indicated. Cleavage of the C3 α chain is indicated by formation of the α' product, and consumption of fB is indicated by appearance of Bb. This experiment was repeated twice.

Supplementary Figure 5

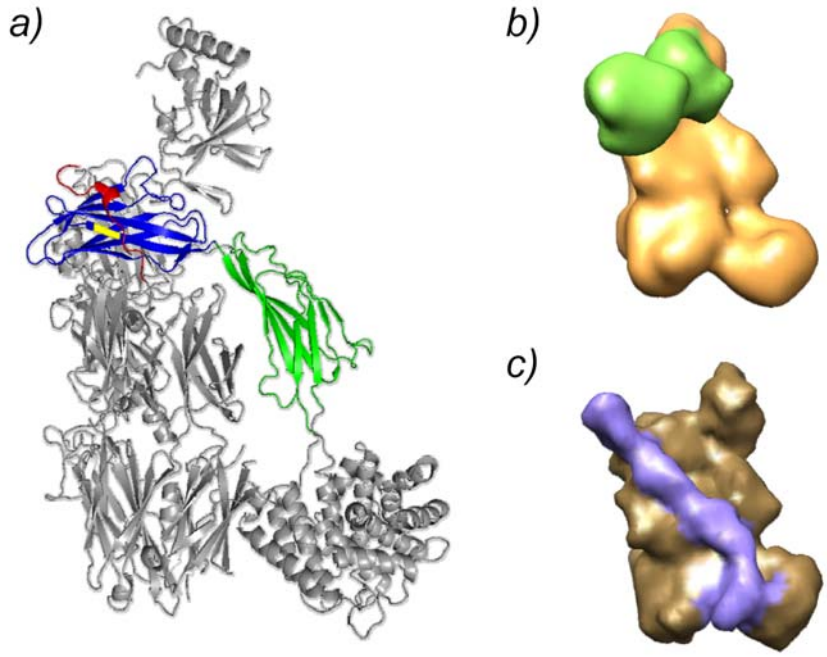

Location of the $C3_{923\Delta DG}$ mutation in C3b.

a) 3D structure of C3b, adapted from Janssen et al. (1), indicating the position of the two amino acids deleted in $C3_{923\Delta DG}$ (yellow) in MG7 (blue). The position of the α'-NT (red) and CUB (green) domains are also indicated.

b) Position of the Bb fragment of fB (green) in the AP C3 convertase C3bBb as described by Torreira et al (2) and Rooijakkers et al. (3)

c) Interaction between fH (blue) and C3b (brown) adapted from Wu et al. 2009 (4).

References:

1. Janssen BJ, Christodoulidou A, McCarthy A, Lambris JD, Gros P. Structure of C3b reveals conformational changes that underlie complement activity. *Nature*. 2006;444(7116):213-6.
2. Torreira E, Tortajada A, Montes T, Rodríguez de Córdoba S, Llorca O. 3D structure of the C3bB complex provides insights into the activation and regulation of the complement alternative pathway convertase. *Proc Natl Acad Sci U S A*. 2009;106(3):882-887.
3. Rooijakkers SHM, Wu J, Ruyken M, van Domselaar R, Planken KL, Tzekou A, Ricklin D, Lambris JD, Janssen BJC, van Strijp JAG, Gros P. Structural and functional implications of the alternative complement pathway C3 convertase stabilized by a staphylococcal inhibitor. *Nat Immunol*. 2009;10(7):721-727.
4. Wu J, Wu YQ, Ricklin D, Janssen BJC, Lambris JD, Gros P. Structure of complement fragment C3b-factor H and implications for host protection by complement regulators. *Nat Immunol*. 2009;10(7):728-733.

Supplementary Figure 6

A model for the interaction between the AP C3 convertase (C3bBb) and its C3 substrate.

We have built a tentative model for the recognition complex between the AP C3 convertase (C3bBb) and its substrate C3 based on the dimeric complexes observed in the crystals of the AP C3 convertase (C3bBb) stabilized with the staphylococcal inhibitor SCIN reported by Rooijakkers et al. (1). As suggested by these authors the interface between two C3b monomers in the crystal likely represents the natural binding interface between C3 and C3b molecules. In the C3b-C3b homodimers, the interface takes place between facing MG rings with main contacts taking place at the level of the MG4 and MG5 domains. Our model was generated by aligning the MG4 and MG5 domains of one of the C3b molecules in the crystals with the atomic structure of C3 (2) using UCSF Chimera (http://www.cgl.ucsf.edu/chimera/). After removing this C3b molecule, the Bb molecule bound to it and the two SCIN molecules included in the Rooijakkers et al. (1) atomic structure, a structural PDB file was saved containing exclusively one C3bBb complex (AP C3 convertase) and the C3 molecule attached to it. This model suggests that apart from the contacts involving MG4 and MG5 domains, the MG7 domains also participate in the interaction between the C3 and C3b molecules. We propose that this binding surface is altered by the $C3_{923\Delta DG}$ mutation.

It should be noted that the region of contact between C3 and C3b involving the MG7 domain may be set slightly apart in the crystal structure reported by Rooijakkers et al. (1) due to the presence of the bacterial inhibitor SCIN. We propose that in normal conditions, in the absence of the inhibitor, the contact interface between C3 and C3b likely involves a tighter interaction at the MG7 region. Therefore, our conclusion from this model is that the $C3_{923\Delta DG}$ mutation alters a region of tight contact between C3b and C3, interfering significantly the interaction between the AP C3 convertase (C3bBb) and its C3 substrate.

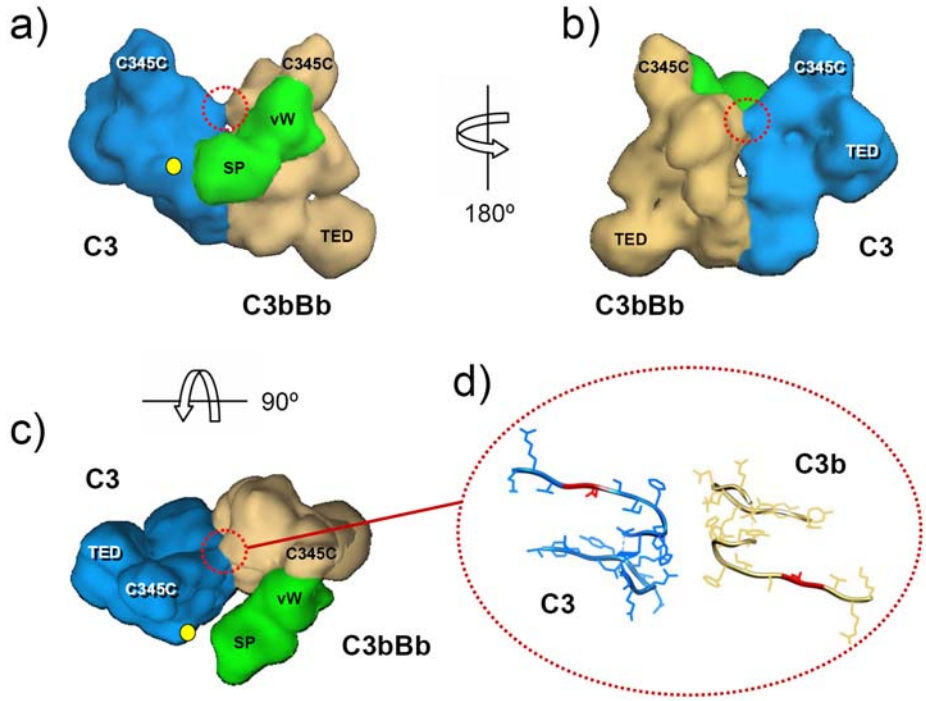

a-c) Three views of the hypothetical C3bBb-C3 complex, where some domains in C3, C3b and Bb are labelled to facilitate the orientation. Code for colours: Blue is C3; Sienna is C3b and green is Bb. The red circle locates the contact between the MG7 regions in C3 and C3b that are likely altered by the $C3_{923\Delta DG}$ mutation. The yellow dot locates the region of C3 where cleavage by the convertase takes place.

e) Close up view of the region of contact between the MG7 domains of C3 (blue) and C3b (sienna) revealing the proximity of this region to the amino acids (Asp923,Gly924) deleted by the $C3_{923\Delta DG}$ mutation (red).

References:

1. Rooijakkers SHM, Wu J, Ruyken M, van Domselaar R, Planken KL, Tzekou A, Ricklin D, Lambris JD, Janssen BJC, van Strijp JAG, Gros P. Structural and functional implications of the alternative complement pathway C3 convertase stabilized by a staphylococcal inhibitor. *Nat Immunol*. 2009;10(7):721-727.
2. Janssen BJC, Huizinga EG, Raaijmakers HCA, Roos A, Daha MR, Nilsson-Ekdahl K, Nilsson B, Gros P. Structures of complement component C3 provide insights into the function and evolution of immunity. *Nature*. 2005;437(7058):505-511.